









Article

Probing the Elastic Scattering Differential Cross Section for Al + p at Backward Angles in a Low Energy Regime

Javier Mas Ruiz ^{1,*}, Karla Gutierrez Zayas-Bazán ², Patricia G. Zayas-Bazán ³, Arcadio Huerta ⁴, Jorge Sastré-Hernández ⁵, Daniel José Marín-Lámbarri ⁴, Luis Acosta ⁴, Eduardo Andrade ⁴, Corina Solís ⁴ and Efrain R. Chávez Lomelí ⁴

¹ Instituto de Ciencias Nucleares, Universidad Nacional Autónoma de México, Cto. Exterior S/N, Mexico City 04510, Mexico

² Unidad Profesional Interdisciplinaria de Energía y Movilidad, Instituto Politécnico Nacional, Mexico City 07738, Mexico; kzayaz@ipn.mx

³ Instituto de Investigaciones en Materiales, Universidad Nacional Autónoma de México, Mexico City 04510, Mexico

⁴ Instituto de Física, Universidad Nacional Autónoma de México, Av. Universidad 3000, Mexico City 04510, Mexico; arcadio@fisica.unam.mx (A.H.); dmarin@fisica.unam.mx (D.J.M.-L.); acosta@fisica.unam.mx (L.A.); andrade@fisica.unam.mx (E.A.); corina@fisica.unam.mx (C.S.); chavez@fisica.unam.mx (E.R.C.L.)

⁵ Escuela Superior de Física y Matemáticas, Instituto Politécnico Nacional, Edificio 9 U.P. "ALM", Mexico City 07738, Mexico; jsastre@ipn.mx

* Correspondence: javier.masruiz91@gmail.com

Abstract: We report on the absolute differential cross section for proton elastic scattering on aluminum in the energy range of 0.8 MeV to 2.1 MeV. In the literature we have found previously published data that follow similar trends but are not consistent with one another. The present measurements also fall within that range, moreover, covering angular regions where there were no reported data, improving databases such as IBANDL. Different methods for the optical model calculations are shown where angular distributions at backward angles are in good agreement, allowing one to fix the optical potential parameters. The calculation results, as well as their data fit, differ significantly as one would expect for the energy range covered in this work, where the nuclear part of the interaction contribution is almost zero. Our data, as well as previous reports, suggest an increase with higher energies for the value of the elastic cross section at backward angles. Further work is required from both experimental and theoretical fronts.

Keywords: elastic cross section; aluminum; RBS; optical model



Citation: Mas Ruiz, J.; Zayas-Bazán, K.G.; Zayas-Bazán, P.G.; Huerta, A.; Sastré-Hernández, J.; Marín-Lámbarri, D.J.; Acosta, L.; Andrade, E.; Solís, C.; Chávez Lomelí, E.R. Probing the Elastic Scattering Differential Cross Section for Al + p at Backward Angles in a Low Energy Regime. *Universe* **2023**, *9*, 438. <https://doi.org/10.3390/universe9100438>

Academic Editor: Maria Benedetta Barbaro

Received: 13 September 2023
Revised: 27 September 2023
Accepted: 28 September 2023
Published: 30 September 2023



Copyright: © 2023 by the authors. Licensee MDPI, Basel, Switzerland. This article is an open access article distributed under the terms and conditions of the Creative Commons Attribution (CC BY) license (<https://creativecommons.org/licenses/by/4.0/>).

1. Introduction

The backscattering (BS) technique is an important tool in materials analysis, as it provides us with an in-depth distribution of the different atomic elements below the surface [1]. The use of protons in this type of study on light targets is becoming more and more common and is preferred over the use of alpha particles. One of the reasons for the above statement is that protons have greater probing depth and higher sensitivity because the effective cross section is enhanced by the nuclear component of the reaction. This proton elastic scattering on light nuclei such as aluminum is dominated by resonances, which result from nuclear potential scattering in addition to the Coulomb interaction [2]. The proton scattering effective cross section by light nuclei at low energies of the order of around 1 MeV is non-Rutherford; therefore, it cannot be calculated with strong precision [3]. It is required to have measurements of the proton scattering effective cross section by light nuclei with the smallest error bars as possible. Numerous proton scattering in aluminum studies have been reported; preceding investigations by Mehta [4] entailed meticulous examinations of proton scattering interactions with aluminum. Their primary aim was to delve into the intricate nuances of nuclear reaction mechanisms. Other investigations of utmost detail

and high resolution were conducted by Nelson [5]. Their measurements encompassed the differential cross sections within an energy spectrum ranging from 0.92 to 3.05 MeV. Notably, these measurements exhibited an exceptional overall resolution, specifically in the range of 350 to 400 eV, and were conducted across various scattering angles. Rauhala [6] investigated proton backscattering in the 1 to 2.5 MeV energy range, with a focus on aluminum and titanium. Their study included rigorous computational analysis in the non-Rutherford energy region at a 170° laboratory scattering angle. Chiari [7] contributed with meticulous proton elastic scattering cross section measurements for aluminum across a broad energy range, from 0.8 to 3 MeV, with an emphasis on backward scattering angles. Ramos [8] determined the aluminum elastic scattering cross sections, spanning the energy range of 0.5 to 2.5 MeV at laboratory angles of 140° and 178° , offering valuable insights into proton-material interactions. Siketic [9] conducted an extensive exploration of proton interactions in the energy range of 2.4 to 5 MeV, with measurements taken at laboratory angles of 120° , 150° , and 165° , contributing to a comprehensive comprehension of proton behavior within this energy domain. Cenja [10] provided a proof that the anomaly at the (p, n) threshold, first observed in the $^{27}\text{Al}(p, p)$ reaction, is a general property of proton elastic scattering on nuclei from the $A = 23\text{--}35$ mass region. Shazad [11] reported a proton elastic scattering cross section on aluminum in the 2.4 to 4 MeV energy range; he correlated the observed resonance structure in the 3 to 4 MeV energy range with possible energy levels in ^{28}Si .

The aforementioned studies are summarized as follows: from [5–9] they have measurements in the range of energies and angles similar to this work. Other studies such as [4,10,12] are more focused on studying reaction mechanisms. We can also find data on proton cross sections in aluminum [11,13], where the data are stored in the IBANDL database [14]. In this paper, we report the differential cross sections obtained from proton scattering in aluminum in the 0.8 to 2.1 MeV energy range and 135° to 170° angular region.

The $p + ^{27}\text{Al}$ system has been studied previously. However, each publication offers data that are not consistent with one another. In addition, there has been no previous effort to extract a nucleus–nucleus optical potential that describes the data well in the energy region of our interest. Our new measurements show the need for even more detailed data to solve the discrepancies between different authors. In addition, they provide a first attempt to extract the appropriate form factors for the nucleus–nucleus potential to be used in optical model calculations.

The optical model has been very useful for understanding the global nucleus–nucleus interaction and describing the elastic scattering of ions, especially at bombarding energies below 10 MeV/nucleon. Most common “optical potential” use “Woods–Saxon” form factors. Their best suited parameter sets for a large variety of projectile–target combinations in a wide range of beam energies have been compiled in [15,16]. In a more recent approach, the São Paulo potential [17] attempts to describe the scattering of heavy nuclei within the optical model, adding a general prescription to produce the optical potentials required for any projectile–target combination. The form factors are obtained from a folding (or double folding) procedure, and the number of adjusting parameters is very limited. This description has proven to be very successful for heavy ($A \geq 4$) projectiles. The experimental facilities, setup, and data analysis are described in Section 2. Section 3 provides the results and discussion, and Section 4 offers some conclusions.

2. Experimental Methods

Proton beams were delivered by the 1 MV tandem accelerator facility model 4110Bo of the Accelerator Mass Spectrometry Laboratory (LEMA) located at the Physics Institute of the National Autonomous University of Mexico (IFUNAM). Pure TiH_2 compound powder is compressed into aluminum cathodes to be introduced into the sputtering negative ion cesium source (SNICS), following Middleton [18], to produce the required beam current at all energies. These cathodes were prepared at the radio-chemistry laboratory of LEMA.

The isotope separator is composed of three parts: a low energy mass spectrometer and a high energy mass spectrometer, which are coupled by a tandem electrostatic accelerator (Cockroft–Walton, see [19,20]). To know the beam final kinetic energy E_c , incident on the target inside the chamber, the accelerator terminal voltage V_t (kV) and the charge state q acquired by the particles after losing electrons are used. The kinematic equation that relates them is E_c (keV) = $E_e + (1 + q)V_t$, where $E_e = 35$ keV, which is the kinetic energy of beam extraction from the ion source.

The aluminum targets were prepared by the evaporation technique in a vacuum glass hood. Inside the hood, two heat sources were located, allowing for the evaporation of two different materials (gold and aluminum) without the need to open the chamber. The deposited film thickness was measured with a highly accurate quartz balance with ± 1 nm uncertainty. The structure of our targets was a 100 nm thick aluminum film covered by a 10 nm gold film. The gold was placed for normalization purposes. In all cases, we used a 12 μ m thick carbon substrate.

2.1. Experimental Set-Up

Four passivated implanted planar silicon (PIPS) detectors were placed on a circular concentric plate with the chamber, having the target and its beam spot at the geometrical center of both the chamber and the detector mounting. A 5 mm diameter collimator was placed in front of each detector to ensure a constant solid angle of 1.364 msr each. The detectors have a separation of 10° from one another. The cross section measurements were performed in one position covering four different angles. In the first runs, 140° , 150° , 160° , and 170° were measured. The mount was rotated for the second runs to measure 135° , 145° , 155° , and 165° . The detector energy resolution was 18 keV, measured as FWHM from the scattered proton peak off the gold layer at 1.5 MeV.

Using 1 ns LEMO cables, the signal from the detectors is connected to the 8-channel MSI-8 preamplifier module from Mesytec (Putzbrunn, Germany), which shapes the output pulse and has a compact box shape. Due to the modular configuration, the types of preamplifier modules can be selected individually for each channel. The MSI-8 is the ideal solution for configurations with a combination of different detectors that require individual bias supply and power ranges. The MSI-8 is powered through a standard SUB-D 9 female connector via Mesytec's MNV-4 module, coupled to the nuclear instrumentation module (NIM) standard. The supply voltage to the detectors is distributed by the Quad 1-kV Bias Supply Model 710 (ORTEC; Oak Ridge, TN, USA) voltage source coupled to the NIM standard and is transferred through the MSI-8. To analyze the signal coming from the detectors, a Phillips Model 7164 (Phillips; Incheon, Republic of Korea) 16-channel analog-to-digital converter (ADC) is used, to which each of the MSI-8 output signals and the trigger signal (Gate) are connected. The ADCs peak looks for the maximum of the incoming pulse (maximum 4 V) during a time window and converts it into a number; this also allows the trigger to be connected in series, which initiates data acquisition on several modules at once with a single trigger signal. The ADCs are powered by the computer aided measurement and control (CAMAC) standard, which is controlled by a peripheral component interconnect (PCI) card in an external computer through an acquisition software based on Labview 2023 Q3, which allows one to record and save the measured data.

The proton beam energies were varied by 50 keV steps, and 20 min runs were taken, with a count rate around 1300 counts per second, to reduce the pile-up effects. The reaction chamber pressure was around 10^{-7} mb; additionally, the accelerator terminal voltage stability was one V in one MV.

2.2. Data Analysis

The calibration of our system was performed as in our previous work [21], where the proton backscattering peaks in the gold layer were used. Figure 1 shows the backscattered proton spectrum at 140° for a 1.5 MeV energy beam compared with a simulation using SIMNRA software (SIMNRA 7.03) [22]. The simulation reproduces the different peaks of

the spectrum corresponding to aluminum, gold, carbon substrate, and a small amount of oxygen contamination resulting from the target manufacturing process.

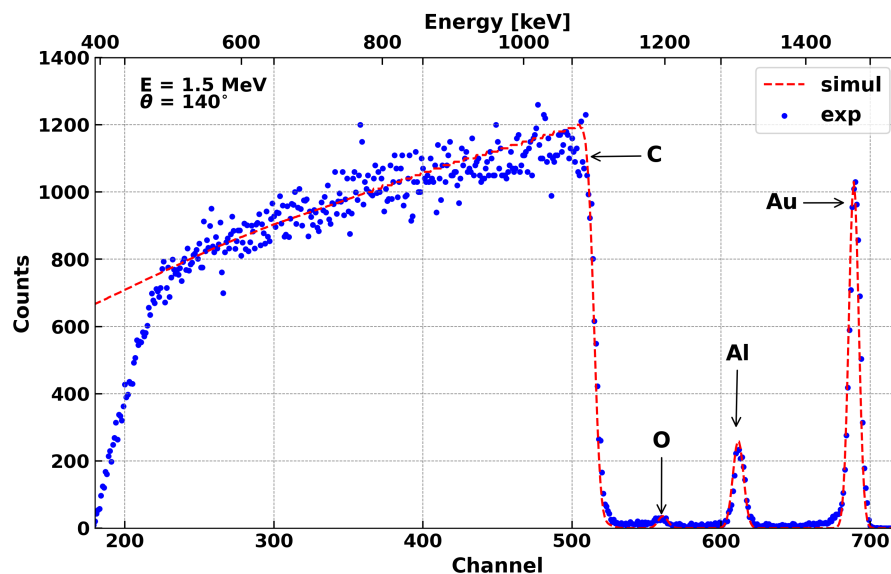


Figure 1. Experimental (blue dots) and simulated RBS spectrum (red dashed line) of 1.5 MeV protons at 140°.

The proton scattering differential cross section in aluminum was obtained from the ratio between the area under the aluminum (A_{Al}) and gold (A_{Au}) peaks, and between the number of atoms per unit area in the gold (N_{Au}) and aluminum (N_{Al}) layer, respectively. This kind of normalization using a gold layer eliminates future corrections for dead time, beam current measurement instability, and solid angle. As can be seen in the formula below:

$$\frac{d\sigma_{Al}}{d\Omega}(E, \theta) = \frac{A_{Al}}{A_{Au}} \frac{N_{Au}}{N_{Al}} \frac{d\sigma_{Au}}{d\Omega}(E, \theta) \tag{1}$$

The energy range for the proton differential cross section in gold for the present measurement is purely Rutherford. The energy value used to report our measured cross sections includes the protons energy loss in the gold and aluminum layers, calculated with the SRIM software (SRIM-2013.e) [23]. The proton energy loss in the 10 nm gold layer ranged from 0.8 keV to 1.3 keV and for the 100 nm aluminum layer ranged from 3.0 keV to 5.4 keV for the minimum and maximum proton beam energy, respectively.

To calculate the differential cross section presented in Equation (1), we need to calculate the N_{Au}/N_{Al} ratio, which gives an idea of the target stability. Its value can be determined from the area under the gold (A_{Au}) and aluminum (A_{Al}) peaks from the RBS spectrum and using Rutherford’s theoretical differential cross section for aluminum and gold. To ensure that the aluminum and gold peaks are the product of purely Rutherford scattering, because the cross section in the low energy regime has an exact analytical expression, the spectra taken in the energy range of 797 keV, 847 keV, 897 keV, 947 keV, and 997 keV (rounded energy values) were used for each measurement angle 135°, 140°, 145°, 150°, 155°, 160°, 165°, and 170°, for which the section should be purely Rutherford, a total of forty spectra (5 different energies x 8 angles each). Already knowing the values of A_{Au} , A_{Al} , $\frac{d\sigma_{Au}}{d\Omega}$, and $\frac{d\sigma_{Al}}{d\Omega}$, the value of N_{Au}/N_{Al} for each selected spectrum can be calculated from Equation (1). The value reported is the average of all calculated values, and the uncertainty is the standard deviation, which gives the measure of the dispersion of the values with respect to the average.

Figure 2 shows the N_{Au}/N_{Al} ratio throughout the whole experiment with an average value of 0.1242 ± 0.0021 , with a stable behavior.

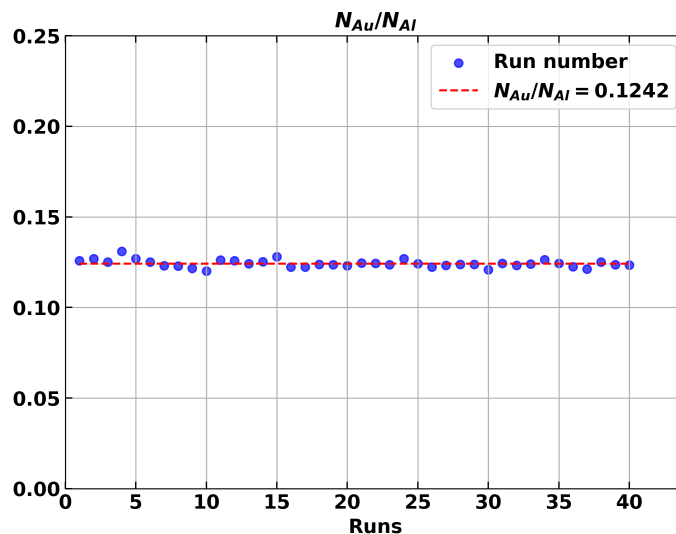


Figure 2. Relation between the number of Au and Al atoms per unit of area for each run number (blue dots) and the mean value (0.124 ± 0.002) in red dashed lines.

3. Results and Discussion

3.1. Differential Cross Section

Here, we present the differential cross section measured in the energy range from 0.8 to 2.1 MeV, normalized to the Rutherford cross section as a function of beam energy (excitation function). In Figure 3, the drawn line in each panel shows the optical model calculation results using an average constant potential with the Woods–Saxon form factor (see next section for the calculation details). Additionally, our data are compared with previous published data in the same energy range. Data are shown for 135° , 145° , 165° , and 170° angles. For all the reported values, the calculated statistical uncertainty was below 5% (except for data taken at 800 keV, 850 keV, and 900 keV, which remained in the range of 5–8%). The experimental data used to compare our results were extracted from the IBANDL database [14].

Figure 3a compares the data measured by Chiari [7] (marked as green x) and Nelson [5] (marked as a blue open circle). Figure 3b and Figure 3c compares the values measured by Chiari [7] (marked as green x), and Figure 3d with those measured by Rauhala [6] (marked as a blue open circle) and Chiari [7] (marked as green x). The measured data are marked as black x in all cases.

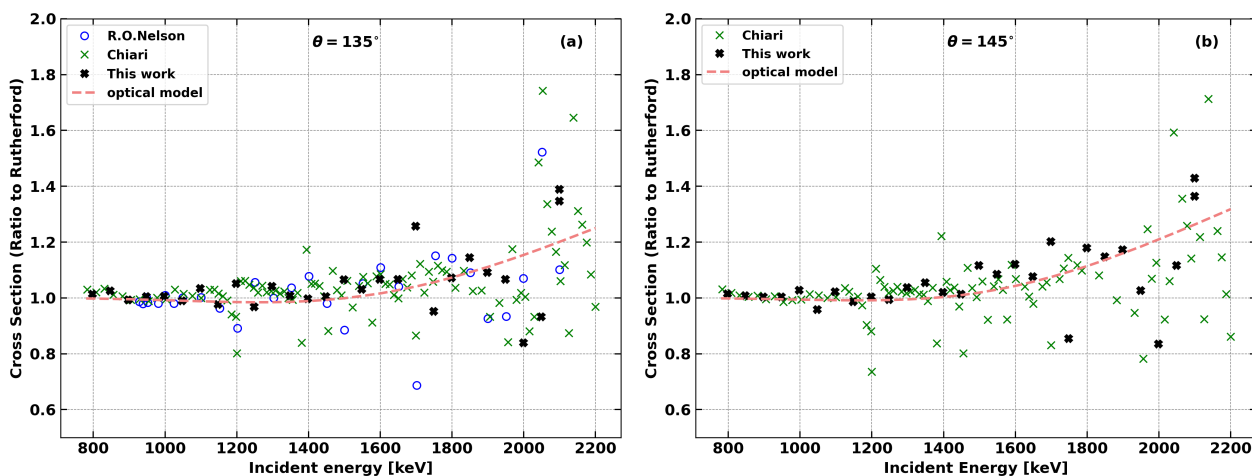


Figure 3. Cont.

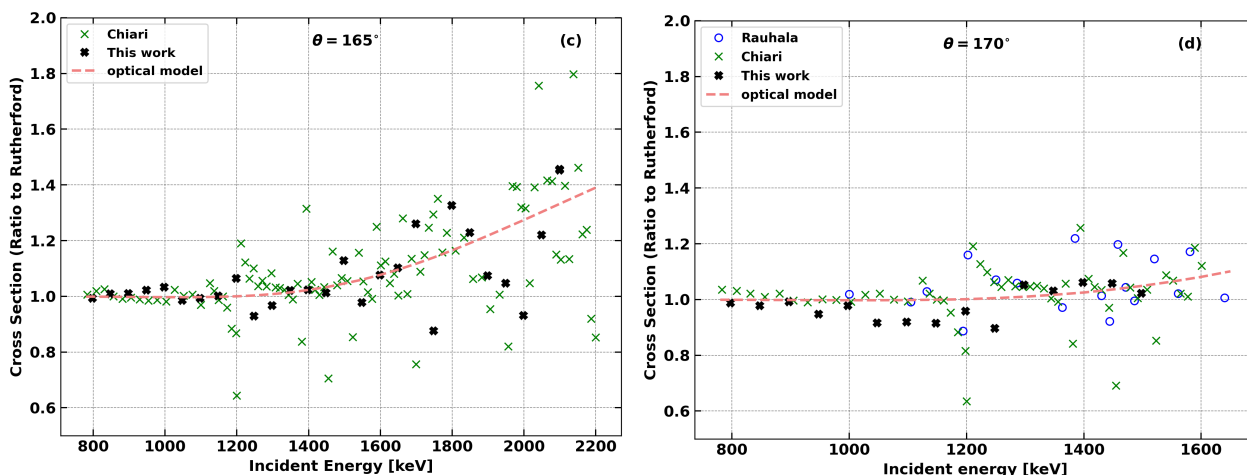


Figure 3. Differential proton elastic cross sections in aluminum normalized to Rutherford at 135°, 145°, 165°, and 170° as a function of bombarding energy. For (a) our data (black filled x) are compared to those in the work by Nelson [5] (marked as a empty blue circle) and Chiari [7] (marked as a green x), for (b,c) we compared with Chiari [7] and for (d) we compared our data with Chiari [7] and Rauhala [6] (marked as a empty blue circle). Red dashed line in each panel shows the optical model calculations.

It is striking how much the data from different authors differ from each other, especially at the forward-most angles. This makes evident the need for an even more thorough study of this elastic cross section. The optical model calculation, which was derived to fit our data, using Woods–Saxon form factors, follows well the general trend of all datasets, becoming a very useful option for ion beam analysis applications. All of our experimental differential cross sections, together with their corresponding statistical uncertainties, are presented in Table 1 and will be uploaded to the IBANDL database [14].

Table 1. Measured differential cross section [†] of (p,p) in aluminum at 135°, 140°, 145°, 150°, 155°, 160°, 165°, and 170°, in the energy range of 0.8 to 2.1 MeV; the values of the cross section and the errors (ε) are reported in the laboratory coordinates system.

E (keV)	135°	ε	140°	ε	145°	ε	150°	ε	155°	ε	160°	ε	165°	ε	170°	ε
796.98	477.62	7.94	440.05	2.11	421.10	7.00	393.49	1.96	383.82	6.38	359.20	1.77	352.62	5.86	344.19	1.68
847.10	427.86	7.11	392.66	2.40	370.28	6.15	348.49	2.07	339.70	5.64	318.69	1.98	317.27	5.27	301.69	1.86
897.22	369.59	6.14	348.29	2.57	328.78	5.46	312.58	2.21	299.18	4.97	288.01	2.02	283.18	4.71	272.88	2.00
947.32	335.38	5.57	306.63	2.62	294.88	4.90	273.21	2.39	268.84	4.47	256.30	2.22	257.09	4.27	233.90	2.09
997.43	302.77	5.03	281.13	2.91	272.41	4.53	251.95	2.60	243.67	4.05	226.06	2.46	234.42	3.90	217.78	2.30
1047.51	270.21	4.49	260.06	2.87	230.46	3.83	228.65	2.51	220.43	3.66	210.79	2.41	202.66	3.37	184.98	2.12
1097.60	257.10	4.27	230.05	3.30	223.92	3.72	206.12	2.93	196.04	3.26	197.89	2.69	186.05	3.09	169.02	2.46
1147.68	222.30	3.69	206.52	3.43	197.65	3.28	183.67	3.05	186.44	3.10	170.88	2.84	171.64	2.85	153.89	2.56
1197.77	219.73	3.65	198.36	3.82	184.57	3.07	176.20	3.42	173.54	2.88	161.91	3.29	167.51	2.78	148.05	2.81
1247.84	186.35	3.10	172.56	4.32	168.42	2.80	150.99	3.80	150.54	2.50	145.21	3.50	134.79	2.24	127.50	3.07
1297.91	185.36	3.08	175.12	4.67	162.49	2.70	156.42	4.19	151.95	2.52	148.12	3.76	129.60	2.25	138.48	3.62
1347.98	166.33	2.76	157.45	5.10	153.14	2.54	144.13	4.54	136.80	2.27	133.82	4.26	126.97	2.11	125.70	3.89
1398.04	152.96	2.54	154.63	5.79	137.71	2.29	132.71	5.19	117.91	1.96	121.55	4.79	118.27	1.97	120.33	4.53
1448.10	143.68	2.39	144.35	6.52	127.53	2.12	124.50	5.79	119.82	1.99	119.13	5.30	109.10	1.81	111.81	1.69
1498.16	142.25	2.36	126.75	7.31	131.19	2.18	117.90	6.54	121.87	2.03	106.64	5.97	113.50	1.89	100.94	5.72
1548.21	128.93	2.14	-	-	119.49	1.99	-	-	102.04	1.70	-	-	92.14	1.53	-	-
1598.27	125.22	2.08	-	-	115.73	1.92	-	-	106.13	1.76	-	-	95.16	1.58	-	-
1648.32	117.63	1.95	-	-	104.58	1.74	-	-	98.56	1.64	-	-	91.62	1.52	-	-
1698.36	130.64	2.17	-	-	109.94	1.83	-	-	104.53	1.74	-	-	98.66	1.64	-	-
1748.41	93.40	1.55	-	-	73.76	1.23	-	-	66.41	1.10	-	-	64.76	1.08	-	-
1798.45	99.41	1.65	-	-	96.25	1.60	-	-	91.47	1.52	-	-	92.64	1.54	-	-
1848.49	100.38	1.67	-	-	88.69	1.47	-	-	84.59	1.41	-	-	81.26	1.35	-	-

Table 1. *Cont.*

E (keV)	135°	ϵ	140°	ϵ	145°	ϵ	150°	ϵ	155°	ϵ	160°	ϵ	165°	ϵ	170°	ϵ
1898.53	90.78	1.51	-	-	85.89	1.43	-	-	72.71	1.21	-	-	67.33	1.12	-	-
1948.57	84.22	1.40	-	-	71.33	1.19	-	-	64.79	1.08	-	-	62.32	1.04	-	-
1998.61	62.97	1.05	-	-	55.20	0.92	-	-	48.76	0.81	-	-	52.67	0.88	-	-
2048.65	66.64	1.11	-	-	70.19	1.17	-	-	59.63	0.99	-	-	65.70	1.09	-	-
2098.68	94.58	1.57	-	-	85.67	1.42	-	-	79.84	1.33	-	-	74.50	1.24	-	-
2098.68	91.65	1.52	-	-	81.73	1.36	-	-	77.06	1.28	-	-	74.68	1.24	-	-

[†] The differential cross section $d\sigma/d\Omega$ and their associated errors (ϵ) are given in (mb/sr).

3.2. Optical Model Calculations

In this section, our optical model calculations performed with FRESKO [24], made to reproduce the values of the measured experimental cross sections, are presented. Data for beam energies of 800 keV, 1300 keV, 1350 keV, 1400 keV, 1450 keV, and 2100 keV are presented as examples of the best fits obtained. Figure 4 shows the Rutherford-normalized experimental cross sections as a function of angle in center of mass coordinates system (angular distributions), as well as the results of the optical model calculations using both Woods–Saxon (WS) and São Paulo (SPP) optical potentials.

It can be seen that calculations using a Woods–Saxon potential follow the experimental normalized Rutherford cross section much better. The theoretical cross section obtained by the calculation has a particular shape, where, for angles between 50° and 100°, a sort of well-like area is observed, and towards angles close to 160°, it starts to increase up to a higher level around 170°–180°. For the SPP case, it fails to reproduce the experimental data; its behavior is much stiffer and behaves like simple Rutherford scattering.

For the Woods–Saxon form factor, we used the parameter set proposed by Koning and Delaroche [15]. This collection of optical parameters for protons is valid over an energy range of ($0 < E < 200$) MeV and for a target nucleon number range of ($24 < A < 209$). Out of the eighteen parameters involved in the recommended form factor of the potential, during the fits, we only varied two of them: the depths of the real (volume) and the imaginary (surface) components.

Table 2 shows the set of parameters varied with their best fit values as a result of our analysis. In addition, the average value used to calculate the excitation functions in Figure 3 is given.

Table 2. Values of the real volumetric (V) and imaginary surface (W_d) parameters for six different beam energies.

Beam Energy (Lab)	V	W_d
800 keV	−58.04	−5.08
1300 keV	−57.83	−5.38
1350 keV	−57.81	−5.41
1400 keV	−57.79	−5.44
1450 keV	−57.77	−5.46
2100 keV	−57.49	−5.82
Average	−57.79	−5.43

In the case of the calculations made using the SPP, the numerical values were generated using a SPOMC [25] program. These values obtained for the SPP were used by the FRESKO code for the calculation of the differential cross sections. The calculations were made with nuclear densities calculated by the SPOMC code, which assumes Fermi–Dirac distributions.

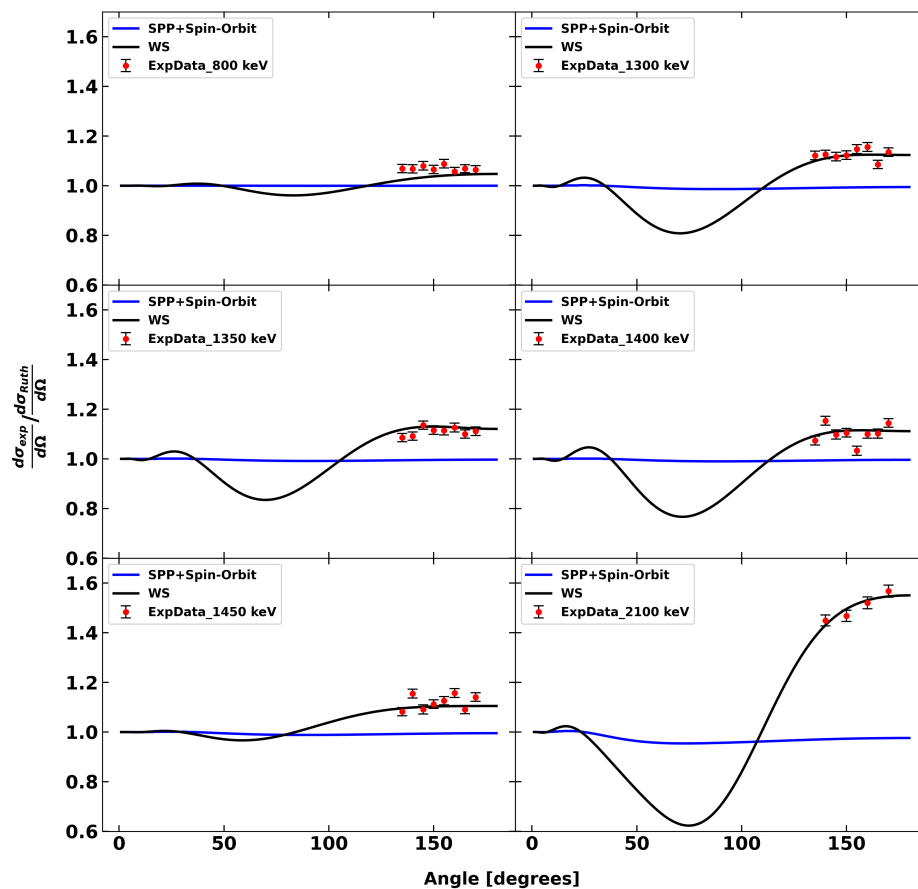


Figure 4. Experimental and theoretical angular distributions relative to Rutherford (center of mass coordinates system). Blue lines refer to the SPP optical potential calculation and a spin-orbit term, and black lines refer to Woods–Saxon optical potential calculations. The experimental error bar was below 3%.

4. Conclusions

In this work, we present the study of proton elastic scattering in aluminum and the differential cross sections at backward angles in the energy region from 0.8 MeV to 2.1 MeV for 8 different angles of 135°, 140°, 145°, 150°, 155°, 160°, 165°, and 170°. These kinds of cross sections are extremely useful for the ion beam analysis of materials (IBA), considering aluminum is commonly used as a thin film or substrate. In that sense, it is very important to count with precise experimental cross sections. Our data improve the reliability of previously published data for this system at similar energies. In addition to the experimental information provided, we also performed an optical potential analysis of our data and a theoretical prescription to calculate these cross sections in a consistent manner for different practical applications. It remains quite evident that a more determined effort has to be made to unify all available data in one coherent set. Further work has to be made as well to improve on the theoretical calculations, specifically, in the definition of a parameter set and form factor for this system at these low energies.

Author Contributions: Writing and draft preparation J.M.R., E.R.C.L. and D.J.M.-L.; targets preparation, K.G.Z.-B. in collaboration with P.G.Z.-B. and J.S.-H.; experimental setup, J.M.R., E.R.C.L., L.A. and A.H.; data taking, J.M.R., E.R.C.L., E.A., A.H., D.J.M.-L. and C.S.; data reduction J.M.R., K.G.Z.-B. and E.R.C.L.; theoretical calculations, J.M.R.; accelerator mentors, C.S. and E.R.C.L. All authors have read and agreed to the published version of the manuscript.

Funding: This work has been partially financially supported by “Universidad Nacional Autónoma de México” research projects under contract numbers: DGAPA-UNAM IG101423 and DGAPA-UNAM IG102023. Posdoc scholarship from National Laboratory (LEMA) foundations.

Data Availability Statement: Experimental data are available on request from Javier Mas Ruiz (javier.masruiz91@gmail.com).

Acknowledgments: The authors are indebted to Sergio Martínez González and Dra. María Rodríguez Ceja for their help and cathodes preparation.

Conflicts of Interest: The authors declare no conflict of interest.

References

1. Chu, W.K. *Backscattering Spectrometry*; Elsevier: London, UK, 2012.
2. Tesmer, J.; Nastasi, M. *Handbook of Modern Ion Beam Materials Analysis*; Materials Research Society: Pittsburgh, PA, USA, 1995.
3. Luomajärvi, M.; Rauhala, E.; Hautala, M. Oxygen detection by non-Rutherford proton backscattering below 2.5 MeV. *Nucl. Instrum. Methods Phys. Res. Sect. B Beam Interact. Mater. Atoms* **1985**, *9*, 255–258. [[CrossRef](#)]
4. Mehta, M.; John, J.; Kerekatte, S.; Divatia, A. Reactions induced by proton bombardment of aluminium. *Nucl. Phys.* **1966**, *89*, 22–32. [[CrossRef](#)]
5. Nelson, R.; Bilpuch, E.; Westerfeldt, C.; Mitchell, G. Proton resonances in ^{28}Si from $E_x = 12.5$ to 13.4 MeV. *Phys. Rev. C* **1984**, *29*, 1656. [[CrossRef](#)]
6. Rauhala, E. Proton backscattering and computer data analysis in the non-Rutherford energy region. *Nucl. Instrum. Methods Phys. Res. Sect. B Beam Interact. Mater. Atoms* **1989**, *40*, 790–796. [[CrossRef](#)]
7. Chiari, M.; Giuntini, L.; Mando, P.; Taccetti, N. Proton elastic scattering cross-section on aluminium from 0.8 to 3 MeV. *Nucl. Instrum. Methods Phys. Res. Sect. B Beam Interact. Mater. Atoms* **2001**, *174*, 259–266. [[CrossRef](#)]
8. Ramos, A.; Paul, A.; Rijniers, L.; Da Silva, M.; Soares, J. Measurement of (p,p) elastic differential cross-sections for carbon, nitrogen, oxygen, aluminium and silicon in the 500–2500 keV range at 140° and 178° laboratory scattering angles. *Nucl. Instrum. Methods Phys. Res. Sect. B Beam Interact. Mater. Atoms* **2002**, *190*, 95–99. [[CrossRef](#)]
9. Siketić, Z.; Radović, I.B.; Skukan, N.; Jakšić, M.; Ramos, A.R.L. Proton elastic scattering from aluminum for 120° , 150° and 165° in the energy interval from 2.4 to 5 MeV. *Nucl. Instrum. Methods Phys. Res. Sect. B Beam Interact. Mater. Atoms* **2007**, *261*, 414–417. [[CrossRef](#)]
10. Cenja, M.; Duma, M.; Hategan, C.; Tanase, M. The (p,n) threshold anomaly in proton elastic scattering on ^{23}Na , ^{27}Al , ^{31}P , ^{35}Cl and ^{34}S . *Nucl. Phys. A* **1978**, *307*, 65–70. [[CrossRef](#)]
11. Shahzad, K.; Qureshi, F.J.; Taj, J.; Awais, A.; Hussain, J.; Akram, W.; Honey, S.; Ahmad, I.; Malik, M. Differential elastic scattering cross sections of protons from Al in 2.4–4.8 MeV energy range. *Nucl. Sci. Tech.* **2016**, *27*, 33. [[CrossRef](#)]
12. Gong-ping, L.; Xiao-dong, Z.; Jin-zhang, X.; Zheng-min, L. Non-Rutherford elastic scattering cross sections for 160° backscattering of 0.96–2.74 MeV protons from aluminum. *J. Radioanal. Nucl. Chem.* **2001**, *250*, 555–558. [[CrossRef](#)]
13. Elliott, R.; Spear, R. Proton scattering from ^{27}Al in the energy range from 3.5 to 11.3 MeV. *Nucl. Phys.* **1966**, *84*, 209–234. [[CrossRef](#)]
14. IAEA. Ion Beam Analysis Nuclear Data Library. Available online: <https://www-nds.iaea.org/exfor/iband1.htm> (accessed on 1 April 2023).
15. Koning, A.; Delaroche, J. Local and global nucleon optical models from 1 keV to 200 MeV. *Nucl. Phys. A* **2003**, *713*, 231–310. [[CrossRef](#)]
16. Perey, C.; Perey, F. Compilation of phenomenological optical-model parameters 1954–1975. *Atoms. Data Nucl. Data Tables* **1976**, *17*, 1–101. [[CrossRef](#)]
17. Chamon, L.C. The São Paulo Potential. *Nucl. Phys. A* **2007**, *787*, 198–205. [[CrossRef](#)]
18. Middleton, R. *A Negative-Ion Cookbook*; University of Pennsylvania: Philadelphia, PA, USA, 1989. Available online: <https://www.pelletron.com/cookbook.pdf> (accessed on 5 February 2023).
19. Cockcroft, J.; Walton, E. Experiments with high velocity positive ions. I.—Further developments in the method of obtaining high velocity positive ions. *Proc. R. Soc. Lond. Ser. A Contain. Pap. Math. Phys. Character* **1932**, *136*, 619–630.
20. Cockcroft, J.; Walton, E. Experiments with high velocity positive ions. II.—The disintegration of elements by high velocity protons. *Proc. R. Soc. Lond. Ser. A Contain. Pap. Math. Phys. Character* **1932**, *137*, 229–242.
21. Reza, G.; Andrade, E.; Acosta, L.; Góngora, B.; Huerta, A.; Marín-Lámbarri, D.; Mas-Ruiz, J.; Ortiz, M.; Padilla, S.; Solís, C.; et al. Characterization of the new hybrid low-energy accelerator facility in Mexico. *Eur. Phys. J. Plus* **2019**, *134*, 590. [[CrossRef](#)]
22. Mayer, M. SIMNRA, a simulation program for the analysis of NRA, RBS and ERDA. In *Proceedings of the AIP Conference Proceedings*; American Institute of Physics: Garching, Germany 1999; Volume 475, pp. 541–544.
23. Ziegler, J. SRIM-2003. *Nucl. Instrum. Methods Phys. Res. Sect. B Beam Interact. Mater. Atoms* **2004**, *219*, 1027–1036. [[CrossRef](#)]
24. Thompson, I. Coupled reaction channels calculations in nuclear physics. *Comput. Phys. Rep.* **1988**, *7*, 167–212. [[CrossRef](#)]
25. Chamon, L. *SPOMC Computational Code, Internal Publication of the Nuclear Physics*; Department of the Physics, Institute of the University of São Paulo: São Paulo, Brazil, 2006.

Disclaimer/Publisher’s Note: The statements, opinions and data contained in all publications are solely those of the individual author(s) and contributor(s) and not of MDPI and/or the editor(s). MDPI and/or the editor(s) disclaim responsibility for any injury to people or property resulting from any ideas, methods, instructions or products referred to in the content.